2D FLOW AROUND STATIONARY SIDE-BY-SIDE SQUARE COLUMNS AT LOW REYNOLDS NUMBER

*Guan Mengzhao [1], Ma Shengwei [3], Francesca Siracusa [2], Kang Chang-Wei [3], *Lim Teck-Bin Arthur [3], Gabriel Weymouth [2], Owen Tutty[2], Tan Mingyi [2], Dominic Hudson [2], Rajeev Kumar Jaiman [3], Wu Chih-Hua [3]*

[1] Department of Mechanical Engineering, National University of Singapore, Singapore
[2] Southampton Marine and Maritime Institute, University of Southampton, Southampton, UK
[3*]Institute of High Performance Computing, A*STAR, Singapore

Abstract: Flow over two side-by-side square columns is studied numerically and experimentally at low Reynolds number (Re=100-200) to investigate the effects of the gap distance on the behavior of the flow. Different gap distances between two square columns are simulated to analyze the interactions of laminar wakes with a gap flow. Four different flow regimes are observed based on different gap distance. Experimental test are performed to validate the simulations. A new water tank has been built specifically for these tests due to the requirements of low Reynolds number and the high sensitivity of the gap flow. Initial experimental flow visualizations of the vortex wake confirm the findings of distinct gap flow regimes.

Keywords: vortex-induced motion; square cylinder; vortex shedding
Article ID: 1671-9433(2010)01-0000-00

1 Introduction

Many engineering applications, such as the offshore structure and civil or industrial buildings, encounter the problem of flow past cylinders. Most of those structures appear as multiple objects. Much work has been done on flow past single object, but less attention has been paid to multi-column problems. This study focuses on flow past two side-by-side identical square columns. A deeper understanding of the behavior of flows past two square columns is essential for engineering application. In this paper the gap ratio g* defines the gap distance between the sides of two square columns, normal to the flow, scaled on the width of the columns. For convenience, all the literature mentioned below will convert their measures of gap ratio into our convention. Kolar et al. (1997) studied the characteristics of a turbulent flow pass two side-by-side identical square cylinders (g* = 2.0) at Reynolds number around 23,100 by using a two-component laser-Doppler velocity-meter system. The work observed a symmetric flow about the central line. The Strouhal number was higher than the one with a single square column. However, the work was done in a near wall condition, which resulted in a vortex speed at the base region significantly higher than in other regions. Shun et al. (2010) conducted experiments in an open-loop wind tunnel, using a smoke-wire method to visualize the flow. The Reynolds number and gap ratio were 2,262 < Re < 28,000 and 0.6 < g* < 12.0, respectively. They classified three different regimes: single mode, gap-flow mode and couple vortex-shedding. The maximum drag coefficient and Strouhal number occurred in the single mode, while the minimum drag coefficient and Strouhal number occurred in the gap-flow mode. Alam et al (2011& 2013) conducted a comprehensive set of experiments on the wake of two side-by-side square columns at Reynolds number about 47,000 and 0 < g* < 5.0. Instead of the three regimes reported by Shun, Alam identified four flow regimes. He divided the gap flow mode into two regimes. At g* = 0.3~1.2, once the gap flow developed sufficient strength, it was biased towards one column, with the wake developing two vortex streets, one narrow and one wide, resulting in one high and one low vortex frequency. This was referred to as two-frequency regime. At g* = 1.2~2.0, (transition regime), three distinct vortex frequencies were detected intermittently with the two-frequency mode.

Only a few works have been found on numerical investigations of two column flow. Numerical computations can eliminate some of the uncertainties occurring in experiment, such as wall boundaries issues in wind tunnels, or the surface roughness of the columns, but can introduce others, notably uncertainties arising through the use of turbulence models at high Reynolds numbers. However, numerical methods can be used without approximation at low Reynolds number to investigate the basic physics of the flow. Sohankar et

al (1999) used a direct numerical simulation method (DNS) to investigate 2D and 3D flow past single square columns at low Reynolds number (Re = 150~500).The shedding flow begins to transition from 2D to 3D in the range of 150<Re<175 (Robichaux et al, 1999). At low Reynolds number the 2D simulations produce drag and lift coefficients that agree well with experiments data. The span-wise extent of the body is important and affects the lift coefficient when the flow becomes 3D. Many numerical simulations only focus on a single square column and do not consider multi-columns system.

Burattini et al (2013) simulated the two side-by-side square columns by using a Lattice Boltzmann method at Reynolds number 73 with gap ratios g* between 0.5 and 6.0. They observed in-phase, anti-phase and quasi-periodic shedding regimes, with a Strouhal number of around 0.16 and a second frequency in the force coefficients at lower g*.

2 Problem Descriptions and Methodology

2.1 Problem Descriptions

Flow past side-by-side square columns at incident angle 0°provides a geometrically simple model of flow past multi-column offshore structures. Fig 1 schematically shows the 2D problem considered here. The side of the square column is fixed at unit length D. The gap length is defined by the distance between two sides of each column and the gap ratio is defined as g* = g/D. The Cartesian coordinate system origin is the mid-point of the line between the two square columns. The distances to the upstream and downstream boundaries are respectively 20D and 40D. At the inlet of domain, a uniform flow is prescribed as (U_∞ = 1, V = 0). At the outlet of the domain, a stress-free condition is imposed. The distance between the outer side of the column and the boundary is kept at S = 19D. A slip boundary condition at the sides of the domain. No-slip is applied at the column surface. A variable gap distance between 0.1D to 10D is used. Two special cases are simulated as references to be compared with the results obtained in the side-by-side system. The first case is the single square column. The second one is characterized by the two side-by-side square columns connected together, acting as one object, with a cross-section of 2D x 1D.

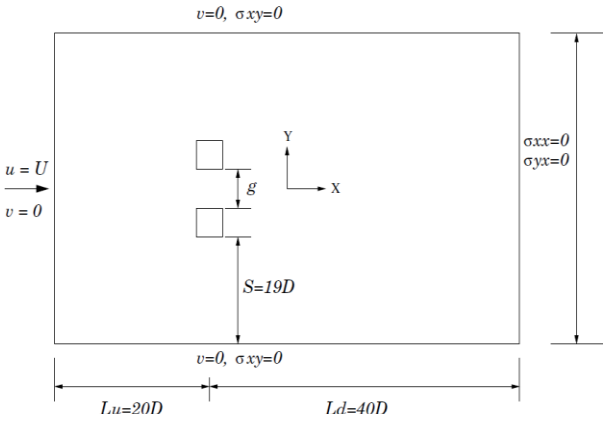

Fig.1 Schematic diagram of flow past side-by-side square columns with boundary conditions

An unstructured, non-uniform finite-element mesh is used in this study. Fifty nodal points are uniformly distributed along each side of the square column. Each element surrounding the columns and in the gap area has a side of 0.02D. A box of 7D x (7D+g) in size surrounds the square columns with a relatively high grid density. For g* = 0.1, 47,874 elements are used (Fig. 2), with 55% of them (26,331) is in the box area, 350 of which are in gap area.

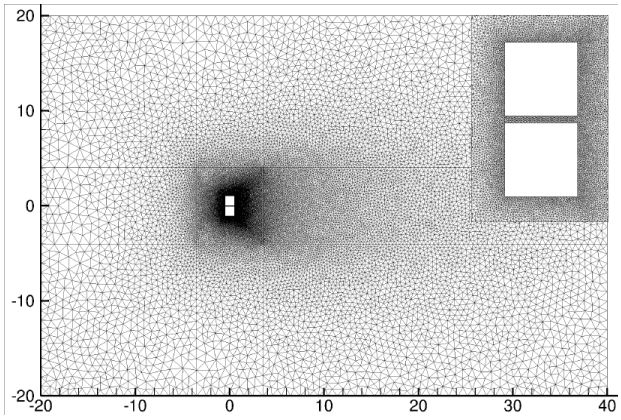

Fig.2 The non-uniform, multi-block, unstructured finite element mesh

2.2 Experimental Methodology

A water tank has been built to experimentally validate the simulations at very low Re, as shown in Fig 3. The tank is composed of four parts: the settling tank, the contraction, the test section and the flow discharge tank. The water enters the settling tank by a hose and exits through a honeycomb. The 6:1 contraction region connects the settling tank to the test section, aligning the flow and bringing it up to speed. The test section is where the cylinders are placed, and the sides and the bottom of this section are constructed of transparent acrylic to enable flow visualization. Finally the water is removed from the flow discharge tank using a second hose. The device that supports two columns is set transverse to the

flow direction and it is equipped with two sliding supports driven by two screws, to set different gaps between the columns. The columns are also made of clear acrylic and the width D is 4mm. The whole device, except for the screws, has been 3D printed. Transfusion tubes are fixed in front of the columns to inject visualization dye. This dye flow is recorded using a camera mounted above the test section.

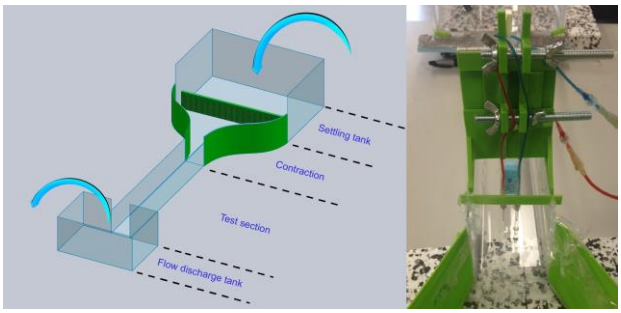

Fig.3 Experimental apparatus. Sketch of the entire flow channel (left), photograph of the cylinder mounting device (right).

3 Convergence and Validation

The grid convergence and the temporal accuracy are discussed in this section. The computational domain used is for g*= 0.1. All the simulations are carried out at low Reynolds number: Re = 200. The viscosity of the fluid, $\mu = \rho UD/Re$, is determined by the Reynolds number used.

3.1 Grid Convergence

Three grids have been generated for mesh convergence studies (Table 1). For the calculations below, grid M2 has been selected because it shows a variation within 1% for the mean drag and RMS value for the lift as compared to the finest grid (M3).

Table 1 Convergence study at Re = 200 and g* = 0.1

	M1	M2	M3
No. of nodes	30,368	52,456	99,778
No. of elements	29,918	51,862	99,024
Averages drag CD	2.5419	2.7114	2.7338
Rms Lift CL	1.1518	1.2122	1.2203

3.2 Temporal Accuracy

The present scheme uses a constant time step. Different time steps $\triangle t$ = 1/10, 1/20, 1/40, 1/80 and 1/100 were investigated (Figure 4) for an associated but more difficult problem, in which the cylinders were allowed to move transversely. A closed-form exact solution for this problem is not available, so a reference solution for $\triangle t$ = 1/200 has been used as the base solution. The amplitude of motion of the cylinder differs by less than 1% when time steps of 1/100 and 1/200 are used (Fig. 4), so a time step of $\triangle t$ = 1/100 was used. Figure 5 shows the second-order accuracy of the time-stepping scheme by plotting the L2 norm of the error against the time step.

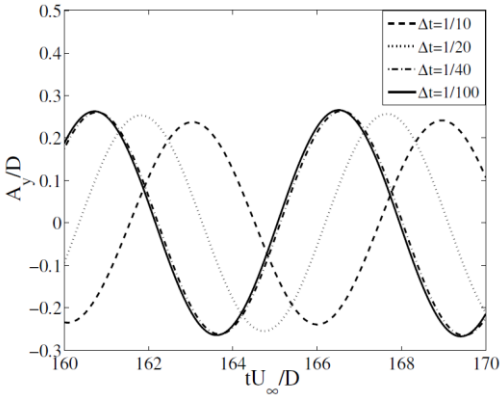

Fig.4 Time step convergence plot for g*= 0.1

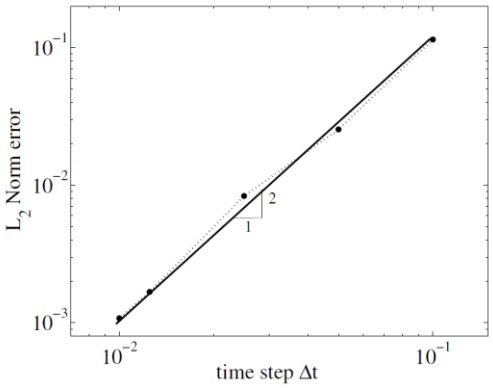

Fig.5 Time step vs L2 Norm Error

4 Numerical Results

Several important non-dimensional parameters are investigated in this study; St (Strouhal Number), C_D (Drag coefficient) and C_L (RMS value of the Lift coefficient).

4.1 Results for validation cases

Two cases were investigated as references to be compared with the side-by-side square columns. The first one consists in the isolated single square column case, where the gap distance is considered as infinity, and the second one is the two square columns case where these are connected together as a single bluff body, with the gap ratio g^* = 0. Unlike a circular cylinder, a square column has fixed separation points of the wake at corners and the flow behavior is less dependent on the Reynolds number. The drag and lift force behaviors of both cases are shown in Fig 6. The flow past a single square column achieves a regular periodic shedding state in around 50 non-dimensional time units, faster than that for g* = 0, which takes 150 non-dimensional time units to settle on its final state. For a single square column C_D = 1.5305, C_L = 0.4899 and St = 0.1465, and for side-by-side connected square columns St = 0.0903. Figure 7 shows that the different cross-section shape also affects the vorticity flow patterns, with a significant gap between the vortices of

opposite sign for the double height configuration as opposed to the more in-line vortex street seen for a single square cylinder.

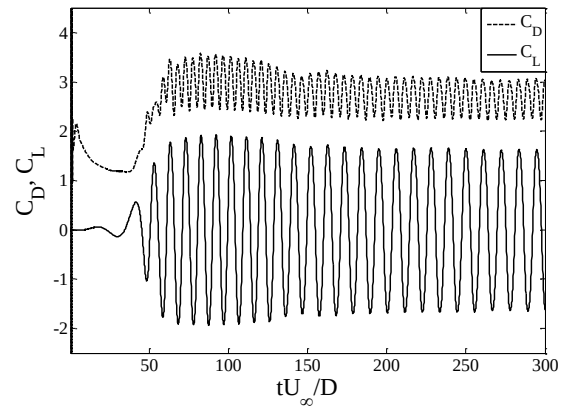

(a) g* = 0

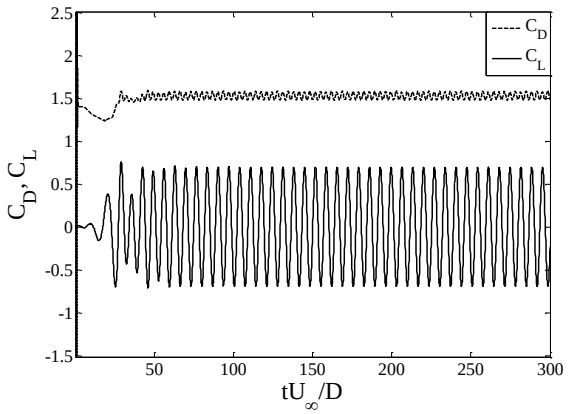

(b) g* = ∞

Fig.6 Time history plot of drag and lift coefficients for the two reference cases: two cylinders touching (a), and a cylinder in isolation (b).

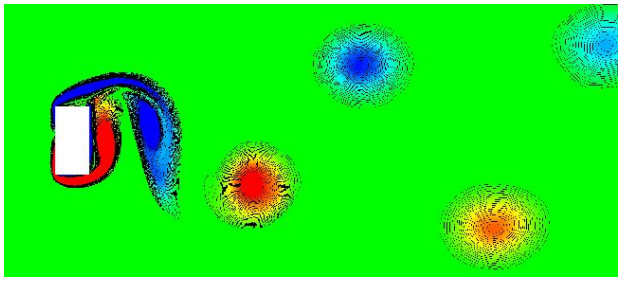

(a) g* = 0

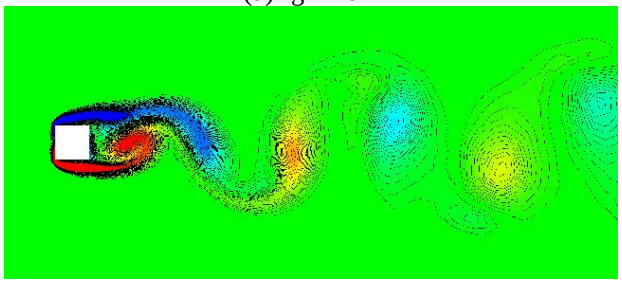

(b) g* = ∞

Fig.7 Vorticity contour plots for reference cases.

In the experiments (Figure 8), initially the flow without obstruction was tested to ensure the quality of the flow in the water tank. Then the two validation cases were investigated for comparison with the previous results. The empty test section case shows that the flow is extremely smooth and unaffected by upstream disturbances. Video of the dye evolution was used to measure the flow in the test section as 0.028 m/s, which was validated by measuring the discharge flow rate. Two validated cases show the expected vortex streets and two-dimensional flows, but the vortex pattern breaks down around 35D, possibly indicating that the dye, slightly more concentrated than the water sinks into the boundary layer. Different gap spacing were tested: g*=0, 1, 2, 3, 5 and 7. The first experiment with g*=0 showed a single vortex street with a vortex spacing of 8D. The experiment using g*=1 showed an asymmetric vortex shedding, and the experiment with g*=2 showed mostly an asymmetric pattern with occasional symmetric behavior. In the experiment with g*=3 the vortex shedding pattern continually switched from the asymmetric mode to the symmetric mode. In both the modes the two rows started merging about 100 mm downstream, forming a single vortex street. At g*=5 the switch between the two modes was continuous and quite slow. At g*=7 one of the cylinders has a lower shedding frequency than the other, missing 4 vortices every 60s.

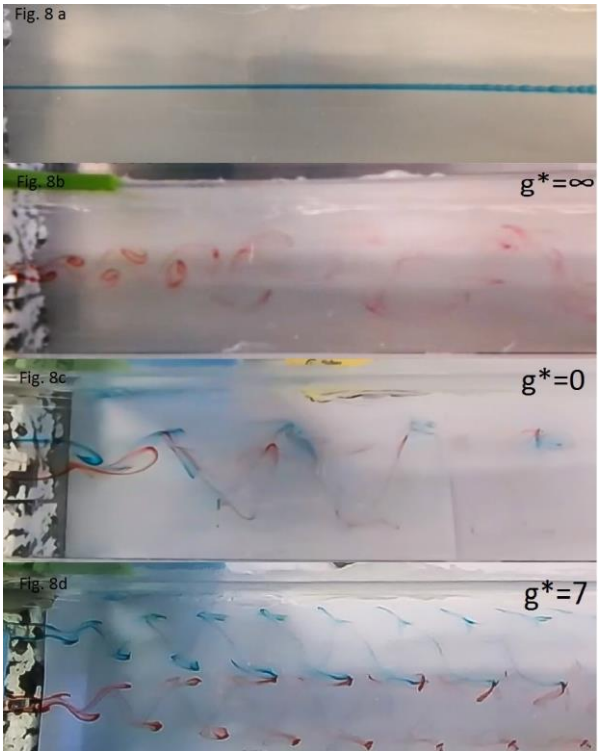

Fig.8 Experimental dye visualization: no bluff bodies (a); single cylinder g*=∞ (b); two side-by-side cylinders g*=0 (c); two side-by-side cylinders with the maximum spacing g*=7 (d).

4.2 Results for the effect of different gap ratio

The cases considered here can be allocated to four different flow regimes (I, II, III, IV) depending on the gap size. With a small gap distance (0 < g* < 0.3,

regime I), the side-by-side system performs as single bluff body similar to the case of $g^* = 0$, with the same lift and drag on each cylinder (Fig. 9). As the gap distance increases ($0.3 < g^* < 2.0$, regime II), the gap flow develops, and there are distinct differences between the mean forces on the cylinders (Fig. 9). For regime III ($2.0 < g^* < 6.0$), the vortex shedding is synchronized, either in-phase or anti-phase. On further increasing the gap, ($g^*>6$, regime IV), the two side-by-side square columns become independent of each other. For regimes III and IV, the mean lift and drag are same on each cylinder (Fig. 9).

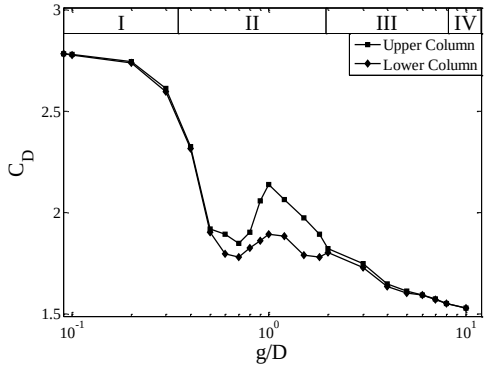

(a) Average of Drag Coefficient for varied g*

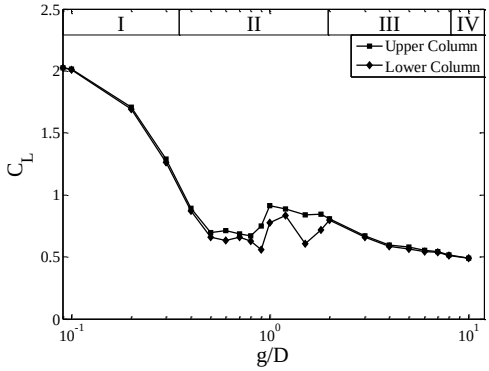

(b) RMS of Lift Coefficient for varied g*

Fig.9 Drag and Lift coefficient for varied g* with the flow regimes indicated.

At $g^* = 0$, no flow passes between the two columns, which act as a single bluff body. At $g^* = 0.1$, a flow forms and attempts to pass through the gap, however, due to the strong shear layer at the back (downstream) surface of the columns, the gap is effectively obstructed by the flow. The change in the flow affects the force on the back surface of the columns, and a second peak appears for every cycle in the drag coefficient. The lift coefficient is the same as at $g^* = 0$. As the gap ratio increases up to $g^* = 0.2$, the gap flow becomes stronger and begins to deflect in the gap area, and, a small peak appears, initially in the lift coefficient plot. As the gap is increased further, the gap flow interacts strongly and dominantly on the back surface; the first peak becomes larger than the second peak, but the total value of the drag coefficient drops (Figures 9 and 10).

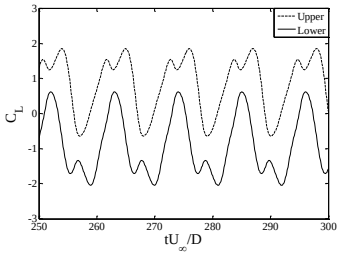

(a)

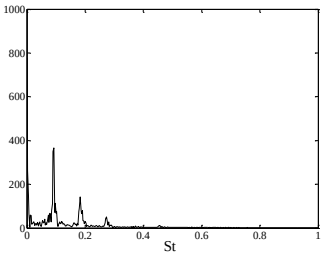

(b)

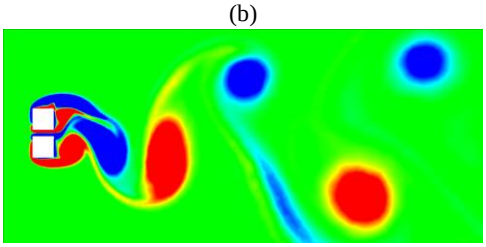

(c)

Fig.10 Flow characteristic of regime I (g* = 0.28): lift coefficient (a), power spectrum (b), and vorticity (c).

After $g^* = 0.4$, the gap flow develops more strongly, enough to split the wake into two streets, a narrow one and a wide one. The gap flow is biased towards one column and forms a narrow street. However, the bias in the gap swaps between two columns. This phenomenon of the shifting bias in the gap flow is commonly referred to as a 'flip-flop' in the literature. This phenomenon is chaotic, characterized by irregular behavior in both the drag and life coefficients. Due to this 'flip-flop' effect, it is difficult to determine the dominant frequency by using fast Fourier transform (FFT) methods (Figure 10b). The two streets strongly interact with each other, but the value of both drag and lift coefficients in the wide streets are higher than those in narrow streets (around 10%). As the gap ratio is increased to $g^* = 1.2$, the gap flow becomes less biased and the two streets become similar to each other instead of one narrow and one wide. In the wake, the vortices fuse into one street (Figure 11).

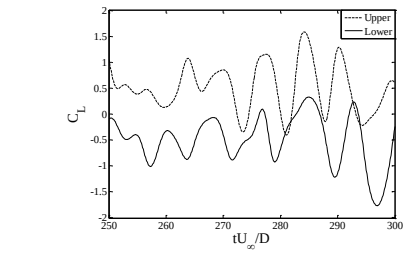

(a)

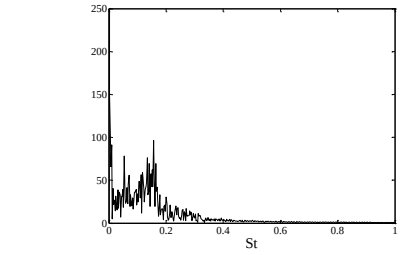

(b)

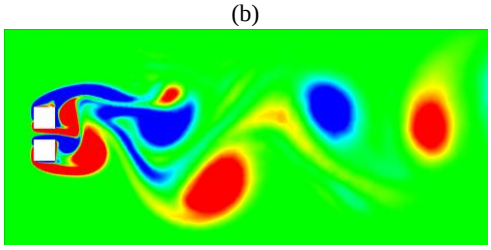

(c)

Fig.11 Flow characteristic of regime II (g* = 0.5)

A transition region where the gap flow is still biased to one side occurs between $g^* = 1.2$ and $g^* = 2.0$ The vortex shedding alternates between in-phase and anti-phase before eventually merging into a single vortex street. For $g^* > 2.0$, the vortex shedding from the two columns is either in-phase or anti-phase. In the anti-phase situation, the flow is symmetric about the center-line of the domain. No interactions between vortices from the different columns are seen in the vorticity contour plot, but the second peak does exist in every cycle in the plot of the drag and lift coefficients. The magnitude of lift coefficient is smaller when the columns are close to each other, while the average values of drag and lift are higher than in the case of a single isolated square column in the reference. When the gap ratio reaches $g^* = 6$, the systems behaves as in the case of the isolated single square column with a difference of the values within 3 %. (Figures 13). In regimes III and IV, again there are distinct peaks in the FTT's corresponding to the shedding frequencies (Figures 12b and 13b).

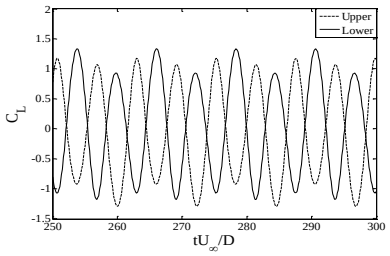

(a)

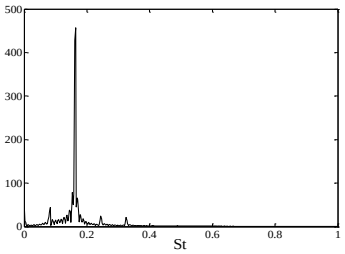

(b)

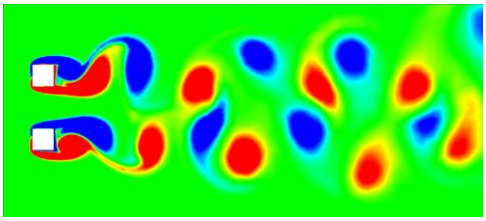

(c)

Fig.12 Flow characteristic of regime III (g*= 2.0).

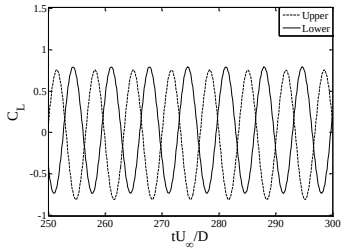

(a)

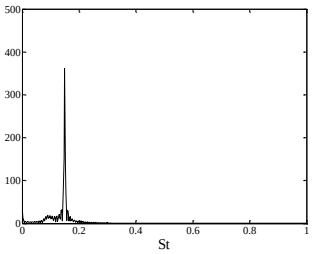

(b)

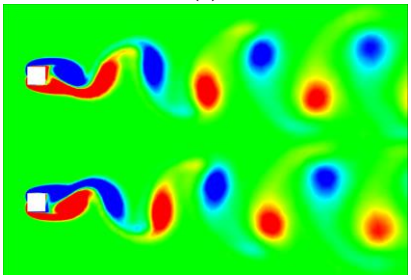

(c)

Fig.13 Flow characteristic of regime IV (g*=6)

4.2 Assessment of the uncertainty of gap flow regime

Two sets of cases were simulated where the inflow flow is varied by a small amount for both $g^* = 0.1$ (regime I) and $g^* = 0.8$ (regime II). Figure 14 shows that a small perturbation in the initial inflow velocity does not change the properties of the lift coefficient in regime I, however, the profiles of lift coefficient are totally irregular for the larger gap. A small change in Reynolds number of this sort would not have a large effect on the flow past a single body for Reynolds number of O(100), so the change in the lift (and flow) can be attributed to the change in the flow in the gap.

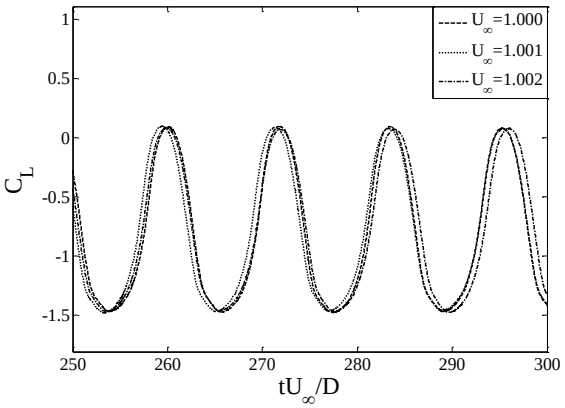

(a) Lift Coefficient plot for g* = 0.1(Regime I)

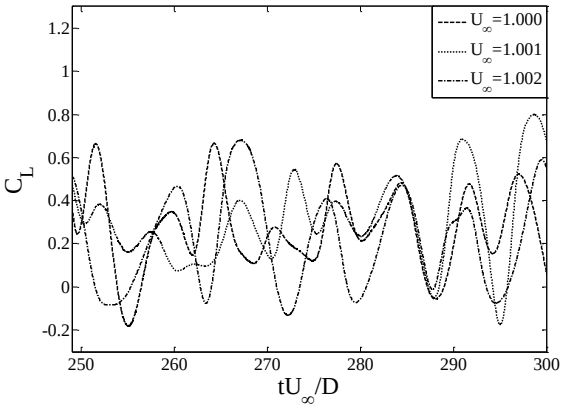

(b) Lift Coefficient plot for g* = 0.5(Regime II)

Fig.14 Assessment of the uncertainty of gap flow regime

5 Conclusions

This paper examines the flow pass two side-by-side square columns at low Reynolds Number 200 with a gap ratio varied between 0 and 10. Four regimes are identified based on different flow behaviors. At flow regime I, also noted as single-bluff-body regime, shear layers only separate alternately from the outer sides of the column; almost no flow passes through the gap and a significant gap flow does not form. All the characteristics are similar to the ones occurring with two connected square columns. As the gap increases, the gap flow develops at the outlet of the gap and it strongly affects the vortex shedding from the columns. The highly irregular nature of the gap flow is tested by changing the initial inflow velocity with a small perturbation. Changing the initial conditions even of 0.1 % can totally modify the behaviour of the drag and lift coefficients. In regime III (or *synchronized*) the vortex shedding is synchronized in either anti-phase or in-phase, which still lightly affect with each other. After the gap ratio exceeds 6, a separated regime occurs (IV) and the two square columns behave as isolated single columns.

In the future, our work will move to study about the freely vibrating columns in two-side-by-sides and four-square-shaped configuration, modelling floating semi-submersible off-shore structures.

References

C. Suqin, G. Ming, H. Ziping (2000), *Numerical Computation of the Flow Around Two Square Cylinders Arranged Side-by-side*, Applied Mathematics and Mechanics vol21

C. Choi and K. Yang (2013), *3D instability in the flow past two side-by-side square cylinders*, PHYSICS OF FLUIDS 25, 074107

M. Alam, M. Moriya, H. Sakamoto (2003), *Aerodynamic characteristics of two side-by-side circular cylinders and application of wavelet analysis on the switching phenomenon*, Journal of Fluids and Structures 18, 325-346

M. Alam, Y. Zhou (2013). *Intrinsic features of flow around two side-by-side square cylinders*, PHYSICS OF FLUIDS 25, 085106

M. Alam, Y. Zhou, XW. Wang (2011), *the wake of two side-by-side square cylinders*, J. Fluid Mech. vol. 669, pp. 432–471

P. Burattini a, A. Agrawal (2013), *Wake interaction between two side-by-side square cylinders in channel flow*, Computers & Fluids 77 (2013) 134-142

J. Robichaux, S. Balachandar, S. P. Vanka (1999) *Three-dimensional Floquet instability of the wake of square cylinder*, Physics of Fluids 11, 560

S. C. Yen, Jung H. Liu (2011), *Wake flow behind two side-by-side square cylinders*, International Journal of Heat and Fluid Flow 32 (2011) 41-51

S. J. Xu, Y. Zhou, R. M. C. So (2011), *Reynolds number effects on the flow structure behind two side-by-side cylinders*, PHYSICS OF FLUIDS VOLUME 15, NUMBER 5

Subhankar Sen, Sanjay Mittal, Gautam Biswas (2010), *Flow past a square cylinder at low Reynolds numbers*, INTERNATIONAL JOURNAL FOR NUMERICAL METHODS IN FLUIDS

V. Kolar, D. A. Lyn, W. Rodi (1997). *Ensemble-averaged measurements in the turbulent near wake of two side-by-side square cylinders*, J. Fluid Mech, vol. 346, pp. 201-237